frontiers in Marine Science

ORIGINAL RESEARCH
published: 11 January 2016
doi: 10.3389/fmars.2015.00117

Studies on Hydroxyl Radical Formation and Correlated Photoflocculation Process Using Degraded Wood Leachate as a CDOM Source

Luni Sun and Kenneth Mopper *

Department of Chemistry and Biochemistry, Old Dominion University, Norfolk, VA, USA

In this study, we examined hydroxyl radical (•OH) formation with respect to photoreactivity of colored dissolved organic matter (CDOM), the Fenton reaction, and photoflocculation using leachate from decaying wood. The relationship between •OH photoproduction rate and leachate optical properties (UV-visible absorption and fluorescence excitation-emission matrices (EEMS)) was studied during irradiation using a UV solar simulator. The results showed that the •OH photochemical formation rate is strongly related to humic-like fluorescence as characterized by parallel factor analysis (PARAFAC), and that these fluorescence components are more photolabile than most of the other CDOM components. Fourier transform infrared spectroscopy (FT-IR) indicated the photodegradation of lignin-related structures. To examine the role of iron and •OH in the photoflocculation process, Fe speciation (particulate Fe, organically-complexed Fe(II), organically-complexed Fe(III), free Fe(II), and free Fe(III)) were measured in the leachate samples amended with Fe. The addition of Fe accelerated •OH production substantially, and Fe was photochemically cycled between Fe(II) and Fe(III). The photodegradation of iron complexing ligands appears to play an important role in DOM photoflocculation.

Keywords: hydroxyl radical, CDOM, EEMS, iron, photoflocculation

OPEN ACCESS

Edited by:
Christopher Osburn, North Carolina State University, USA

Reviewed by:
Cristina Sobrino, University of Vigo, Spain
Leanne C Powers, Skidaway Institute of Oceanography, USA

***Correspondence:**
Kenneth Mopper
kmopper@odu.edu

Specialty section:
This article was submitted to Marine Biogeochemistry, a section of the journal Frontiers in Marine Science

Received: *29 September 2015*
Accepted: *14 December 2015*
Published: *11 January 2016*

Citation:
Sun L and Mopper K (2016) Studies on Hydroxyl Radical Formation and Correlated Photoflocculation Process Using Degraded Wood Leachate as a CDOM Source. Front. Mar. Sci. 2:117. doi: 10.3389/fmars.2015.00117

INTRODUCTION

The hydroxyl radical (•OH) is a highly reactive oxygen species that is formed by photochemical reactions in natural waters (Buxton et al., 1988; Vaughan and Blough, 1998). It not only reacts with a variety of organic and inorganic compounds, but can also impact aquatic organisms, i.e., damaging cells and inducing excretion of protective slime (Mague et al., 1980; Zlotnik and Dubinsky, 1989; He and Häder, 2002). The photo-Fenton reaction and dissolved organic matter (DOM) photoreactions are two of its major sources (Mostofa et al., 2013). In seawater and high DOM freshwaters, DOM photoreactions appear to be the main source for •OH. There are two known •OH production pathways from DOM: a H_2O_2 dependent pathway where the H_2O_2 is formed from DOM (Vione et al., 2006), and an H_2O_2 independent pathway (Page et al., 2011). In the latter pathway, the sources and mechanisms of •OH photoproduction from DOM are still unknown.

In the photo-Fenton reaction, Fe(II) reacts with H_2O_2 to yield •OH and Fe(III). The latter is then reduced to Fe(II), mainly through ligand to metal charge transfer (LMCT) reactions with DOM (Scott et al., 1998; Klapper et al., 2002; Barbeau, 2006), and through the reduction by HO_2/O_2^- (Voelker et al., 1997). Both inorganic and organically-complexed Fe(II), in which the Fe is usually bound to the phenolic and carboxyl groups (Baruah et al., 1981), take part in the Fenton reaction. Although organically-complexed Fe(II) is less reactive with H_2O_2 than inorganic Fe(II) (Miller et al., 2012), it is environmentally important because •OH may not be produced from the oxidation of inorganic Fe(II) under circum-neutral conditions (Miller et al., 2012), and the inorganic Fe(II) concentration is a small percentage of total Fe (Emmenegger et al., 2001; Shiller et al., 2006).

Several studies have shown that Fe and DOM photochemistries are involved in the photoflocculation process (Zepp et al., 1992; Gao and Zepp, 1998; Helms et al., 2013a), which may be important in transformation and transportation of DOM and particulate organic matter (POM) from rivers to the ocean (Helms et al., 2013a; Chen et al., 2014). Gao and Zepp (1998) reported that dark-colored particles formed in river samples after 3 days irradiation, and that the particles accounted for 45% of the total iron and 13% of the total organic carbon. Kopáček et al. (2005) proposed the photoflocculation pathway proceeds by iron mediated photodegradation of organic iron-binding ligands causing release of inorganic iron to form insoluble hydroxides. Chen et al. (2014) further confirmed that the DOM-associated Fe is converted to insoluble Fe(III) oxyhydroxides. Shiller et al. (2006) showed that organically-complexed Fe is released during photo-oxidation of low molecular-weight DOM, followed by precipitation of the released Fe as colloidal Fe(III) oxyhydroxides.

It is currently not known if •OH produced from DOM and Fenton reactions plays a role in photoflocculation processes. Therefore, a major goal of this study was to examine •OH formation with respect to the Fenton reaction and DOM photoreactions and to determine their potential impact on photoflocculation. We estimated time-course •OH photo-formation rates in Fe-poor leachates of decayed wood using near-instantaneous •OH formation rates. We chose to study wood leachate because it can be an important source for DOM in natural waters (Kalbitz et al., 2000; Spencer et al., 2008; Sun et al., 2014), contains colored DOM (CDOM), and very low iron concentrations. The latter is important because it allowed the effects of added Fe to be readily examined. To elucidate the possible sources for •OH photochemical formation from DOM, DOM optical properties, i.e., UV–visible absorption spectra, specific UV absorption (SUVA), fluorescence excitation-emission matrices (EEMS), and Fourier transform infrared spectroscopy (FT-IR), were measured for the irradiated Fe-poor wood leachate. Furthermore, to study the role of •OH and iron in the photoflocculation process, Fe speciation (particulate Fe, organically-complexed Fe(II), organically-complexed Fe(III), free Fe(II), and free Fe(III)) was measured in the irradiated sample with Fe addition.

EXPERIMENTAL SECTION

Materials

Phenol (purity grade >99%), benzene (HPLC grade), ferrozine (97%), hydroxylamine hydrochloride (%), ammonium acetate (99%), sodium acetate (99%), and ferric chloride (99%) were obtained from Sigma-Aldrich; the iron standard solution was made from ferric nitrate in 2 % (v/v) nitric acid (1000 ppm, Certified, Fisher Chemical), and ferrous ammonium sulfate hexahydrate was obtained from Fisher; methanol (HPLC grade) was obtained from Acros; and Maxi-Clean 600 mg SCX cation solid phase extraction (SPE) cartridges were obtained from Grace. Ultra-pure water (Milli-Q water) was used for solution preparation. All glassware was acid soaked and pre-combusted (450°C).

Sample Description

The decayed wood sample was collected near Portsmouth Ditch in the Great Dismal Swamp (Chesapeake VA, USA). This area is covered by mainly maple gum (http://www.usgs.gov/climate_landuse/land_carbon/default.asp). A high S/V ratio (2.8), defined as the total mass of syringealdehyde, acetosyringone, and sryingic acid divided by the total mass of vanillin, acetovanillone, and vanillic acid measured by CuO HPLC method (Sun et al., 2015a), indicated that the wood sample is angiosperm (Hedges and Mann, 1979). The sample was visually highly degraded. The sample was oven-dried at 60°C for 24 h, crushed into powder by a mortar and pestle to pass through a 600 μm sieve, then a 5.0 g sample was leached in 1.0 L Milli-Q water by continuous mixing overnight at room temperature. The particles were removed by filtration through a pre-combusted 0.7 μm GF/F filter (Whatman), followed by a 0.1 μm capsule filter (Polycap TC, Whatman). Dissolved organic carbon (DOC) and total dissolved nitrogen (TDN) were 12 ppm and 0.5 ppm, respectively. The pH of the wood leachate was 4.3. To examine the effect of iron on the •OH formation rate, 20 μM $FeCl_3$ (final concentration) was added to an aliquot of wood leachate, and the pH was adjusted to the original pH of 4.3. Such high iron concentrations are typical of many DOM-rich natural waters, such as found in the Satilla River and Estuary and the Great Dismal Swamp (White et al., 2003; Chen et al., 2014; Sun et al., 2014). The sample was kept in the dark for 24 h to complete organic-iron complex interaction, and then filtered with a GF/F filter.

Irradiations

The iron unamended and amended samples were placed into 500 mL round-bottom quartz flasks in duplicates. The samples were kept oxygenated by periodic shaking in air, and were irradiated at 22 ± 2°C using a solar simulator. The solar simulator provided 127% of DOM photobleaching occurring under winter mid-day natural sunlight at 36.89°N latitude, which was described elsewhere (Minor et al., 2007; Sun et al., 2014). Some flasks were wrapped in foil and kept as dark controls. At each time point, irradiated and dark control samples were subsampled. •OH formation rates, pH, absorbance, EEMS and Fe speciation (particulate Fe (PFe), organically-complexed Fe (OFe), free Fe (FFe), Fe(II), and Fe(III)) were measured immediately.

The subsamples for DOC/TDN were acidified and stored (4°C) for later analysis. The subsamples for FT-IR analysis were freeze-dried.

•OH Formation Rates

Benzene was used as the •OH probe because it has a higher selectivity than other commonly used probes, such as benzoic acid (Vione et al., 2010). The •OH formation rate at each test time point was determined by irradiating 30 mL subsamples in quartz tubes in the presence of the benzene probe (3 mM) for ≤2 h. This method yields a more accurate estimate of the •OH formation rate than leaving the probe in the sample for the entire irradiation period (Sun et al., 2014). DOC loss was measured in one tube with no probe in order to calibrate •OH formation rates in the tube relative to the round-bottom flask.

The •OH formation rate R was calculated as:

$$R = \frac{R_{ph} \times F}{Y}$$

Where R_{ph} is the observed photo-formation rate of phenol from the reaction of •OH with benzene, which was measured by HPLC; Y is the yield of phenol formed per benzene molecule oxidized by •OH; we used the value of 69.3 ± 2.2% (Sun et al., 2014); F is a calibration factor, which was evaluated by competition kinetics using a series of different benzene concentrations as described in detail by Zhou and Mopper (1990).

Dissolved Organic Carbon (DOC) and Total Dissolved Nitrogen (TDN)

DOC and TDN were measured using high temperature (720°C) catalytic combustion on a Shimadzu TOC-V-CPH carbon analyzer. Potassium hydrogen phthalate (KHP) and KNO_3 were used to make calibration curves to quantify the DOC and TDN concentrations respectively.

Optical Properties

UV–visible absorption spectra were measured by UV-vis absorbance (200–700 nm in 1-nm intervals) using an Agilent 8453 diode array spectrophotometer with a 1 cm quartz cuvette (Helms et al., 2008). Strongly absorbing samples were diluted prior to measurement to ensure linear response. First derivative UV–visible absorption spectra were obtained as described in Helms et al. (2014). $SUVA_{254}$, $SUVA_{280}$, and $SUVA_{300}$ were determined by dividing the absorbance at 254, 280, and 300 nm respectively by the DOC concentration.

Fluorescence EEMS were measured as described in Murphy et al. (2010). Raw EEMS were collected using a Cory Eclipse fluorometer with a 1 cm quartz cuvette at specified excitation wavelengths (λ_{ex}) of 240–450 nm in 5-nm intervals and emission wavelengths (λ_{em}) of 300–600 nm in 2-nm intervals; blank EEMS and Raman scans (λ_{ex} = 350 nm, λ_{em} =365–450 nm in 0.5 nm intervals) were obtained from Milli-Q water, and emission scans (λ_{ex} = 350 nm) were obtained from a quinine sulfate (QS) dilution series (0, 20, 50, 100 ppb) from a 1000 ppb working solution. Data was processed in MATLAB using the FDOMcorr toolbox (Murphy et al., 2010). EEMS were processed by spectral correction, inner filter correction, Raman correction, and QS calibration, and then analyzed by PARAFAC using the DOMFluor toolbox (Stedmon and Bro, 2008). Fluorescence intensity is reported in Raman units (RU) (Murphy et al., 2010).

FT-IR analysis was conducted as described in Abdulla et al. (2010). One milligram sample was mixed with 100 mg pre-heated KBr and homogenized by a Wig-L-Bug grinding mill. Subsamples were then compressed by anvils to a disk. FT-IR spectra were collected using a Nicolet 370 FT-IR spectrometer equipped with purge gas generator unit. Spectra were collected with 200 scans and a resolution of 4 cm^{-1}. The FT-IR spectra were normalized to the integrated absorbance from 4000 to 500 cm^{-1} and multiplied by 1000 in order to account for minor concentration variations between samples. The FT-IR absorbance spectra were processed using OMNIC software with the second-order Savitzky–Golay method with 11 convolution points used to generate the second derivative of the spectra (Abdulla et al., 2010).

Iron Speciation

Fe speciation includes dissolved total Fe (DTFe), particulate total Fe (PTFe), dissolved strong organically-complexed Fe (OFe), and free Fe (FFe). Sub-samples were taken at different time points during the irradiation and 0.2 μm filtered (Gelman Sciences). PTFe was measured indirectly by subtracting DTFe at each time point from the initial DTFe. The FFe and OFe fractions were separated by SCX cation exchange cartridges (Tangen et al., 2002). SCX cartridges were employed because they are more convenient than loose resin (Tangen et al., 2002; Shiller et al., 2006). The cartridges were conditioned with 14 mL Milli-Q water, followed by 14 mL 0.4 M ammonium acetate buffer pH 4.5, and 4 mL of sample to rinse out the buffer. Since FFe is selectively bound to the SCX cartridges, the remaining Fe in eluate solution after SPE extraction was considered as OFe. FFe was calculated by subtracting the Fe concentration after SPE (OFe) from DTFe.

Fe(II) and Fe(III) were determined before and after SPE extraction by a modified ferrozine method (Viollier et al., 2000). Non-reduced sample absorbance for Fe(II), was measured by mixing 5.0 mL of sample, 500 μL 0.01 M ferrozine solution (prepared in 2 M ammonium acetate), 200 μL 5 M ammonium acetate, and standard addition with a range of 0–20 μM. The final pH was 5–6. DTFe was measured after reducing the sample by hydroxylamine hydrochloride (prepared in 2 M HCl). The dissolved Fe(III) concentration was calculated by subtracting Fe(II) from DTFe.

RESULTS AND DISCUSSION

•OH Formation Rates

During irradiation, the •OH formation rate was initially markedly higher in the presence of added Fe (**Figure 1A**). During the first hour, the •OH formation rate reached 1.3 μM/h in the Fe amended sample, which was about five times that of the original (unamended) sample (0.25 μM/h). However, in the Fe amended sample, the •OH formation rates dropped quickly with the occurrence of photoflocculation. Since each sample was run in duplicate, pooled relative standard deviation and pooled numbers (all eight time points) were used for statistical

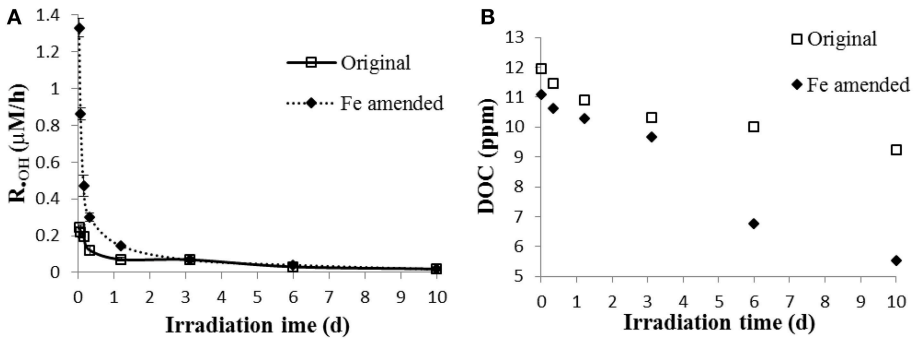

FIGURE 1 | (A) •OH formation rates; **(B)** dissolved organic carbon (DOC) in original and Fe amended aqueous leachates of degraded wood. The •OH formation rate was the mean value calculated from two measurements, and the error bars represent the range.

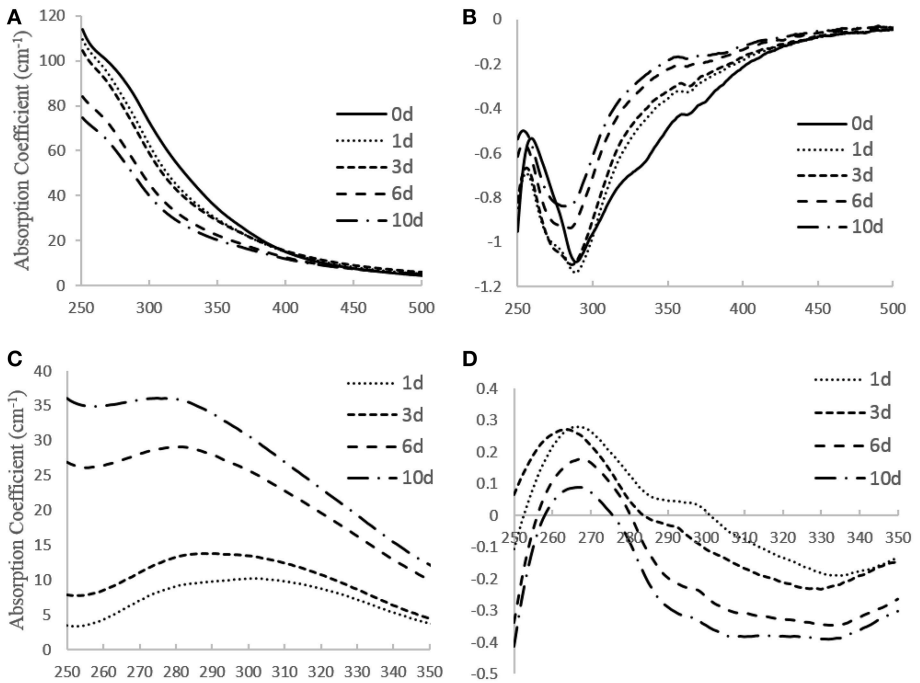

FIGURE 2 | (A) UV–visible absorption spectra, **(B)** first derivative absorption spectra, **(C)** difference spectra, **(D)** first derivative of difference spectra obtained for wood leachate during irradiation.

analysis. The difference in •OH formation rate between the Fe amended and unamended sample was significant during the first 2 days, and insignificant after day 3 (t-test, $p < 0.01$). DOC decreased faster in Fe amended sample than in the original sample. The DOC dropped by 23% in original sample, but 53% in Fe amended sample after 10 d of irradiation (**Figure 1B**), which indicates that Fe-associated photoreactions assist the mineralization, transformation and flocculation of DOM (Pullin et al., 2004; Molot et al., 2005).

Optical Properties of Wood Leachate

From the UV–visible absorption spectra (**Figures 2A,B**), the steepness of the first derivative absorption spectrum around 280 nm decreases with increasing irradiation time (**Figure 2B**). This trend indicates that the short wavelength absorbing chromophores at ∼280 nm, which are likely aromatic chromophores, are preferentially lost. This conclusion is supported by the slope ratio (S_R), which increased from 0.73 to 1.0 during the initial 8 h and stayed at ∼1.0 for the remaining 10 days. An increase in slope ratio indicates loss of aromaticity (Helms et al., 2008). Moreover, the shift to the shorter wavelengths in the minimum in the first derivative spectrum during irradiation (**Figure 2B**), suggests that the degree of conjugation and/or molecular size also decreased during irradiation (Helms et al., 2008, 2013b). Difference spectra (**Figure 2C**) indicates that during the first day of the irradiation,

when •OH production was greatest (**Figure 1**), maximum photobleaching occurred at ∼300–310 nm, as clearly indicated by the first derivative of the difference spectra (**Figure 2D**). Photobleaching then shifted to DOM chromophores that absorbed at ∼270–280 nm as the irradiation progressed (**Figures 2C,D**). These results suggest that chromophores absorbing at ∼300–310 are more photolabile than the remaining chromophores and that they may be mainly responsible for the initially high •OH production, as is supported by past studies (Vaughan and Blough, 1998; White et al., 2003) that showed the highest •OH apparent quantum yield is at 310 nm.

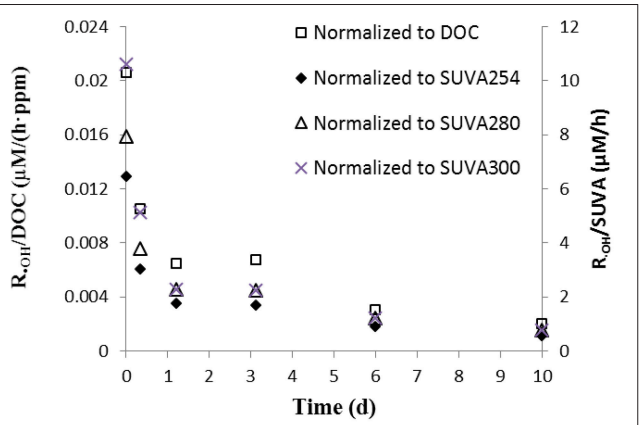

FIGURE 3 | •OH formation rate normalized to DOC and $SUVA_{254}$ in the aqueous leachate of degraded wood.

However, •OH formation rates normalized to DOC, $SUVA_{254}$, $SUVA_{280}$, and $SUVA_{300}$ decreased during the irradiation (**Figure 3**), indicating that •OH production is not simply correlated to DOC and absorbance. Also, the results indicate that the non-irradiated sample had the highest capability of photoproducing •OH, and that the chromophoric sites within DOM responsible for •OH production were preferentially transformed and/or degraded (relative to the total aromaticity) during irradiation, and thus appear to be more photolabile, in agreement with the photobleaching results discussed above.

Fluorescence EEMS showed that the overall fluorescent intensity of the sample decreased markedly during irradiation (**Figure 4**). Three main fluorescent components were characterized in the sample by PARAFAC analyses (**Figure 5**): components 1 (ex/em <250, 305/418) and 2 (ex/em 260, 340/460) are characterized as humic-like DOM (Fellman et al., 2010; Guo et al., 2011), while component 3 is characterized as tryptophan-like DOM (ex/em < 250, 280/350; Yamashita et al., 2008; Fellman et al., 2010; Guo et al., 2011). Components 1 and 2

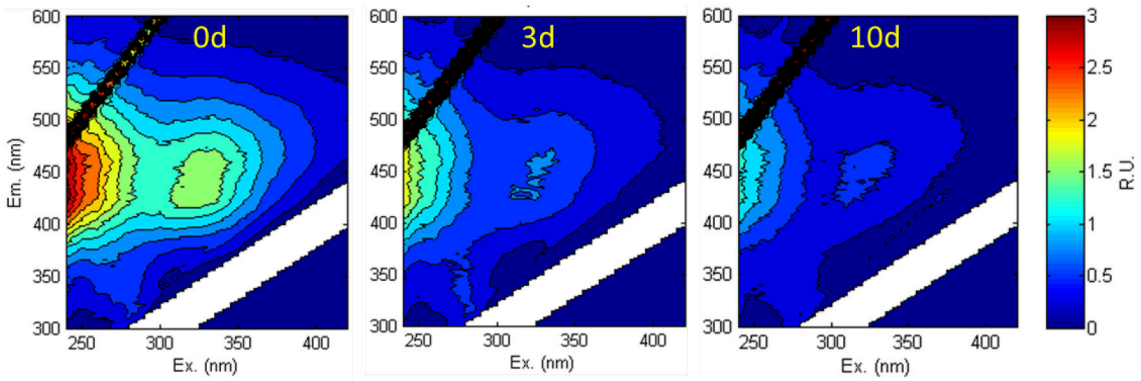

FIGURE 4 | Fluorescence EEMS of the aqueous leachate of the degraded wood sample at 0, 3, and 10 d irradiation.

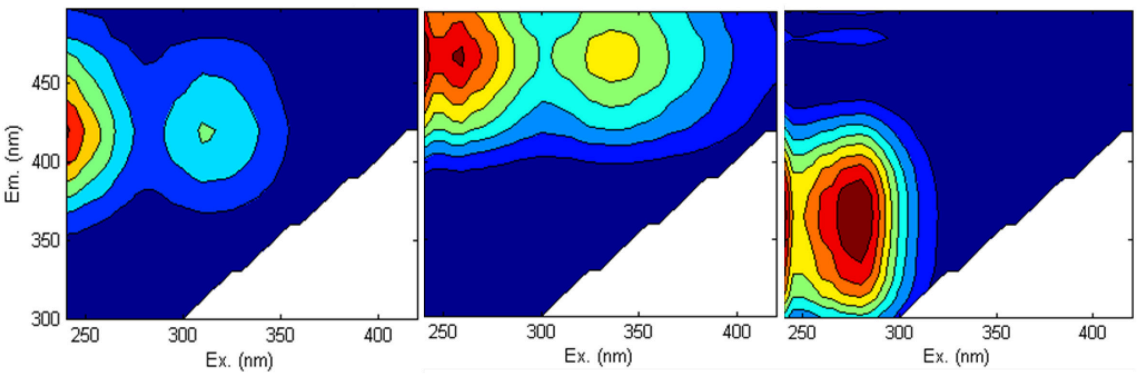

FIGURE 5 | Three components identified by PARAFAC analysis in all non-Fe-amended samples. Components 1 and 2 are humic-like DOM, and component 3 is tryptophan-like DOM.

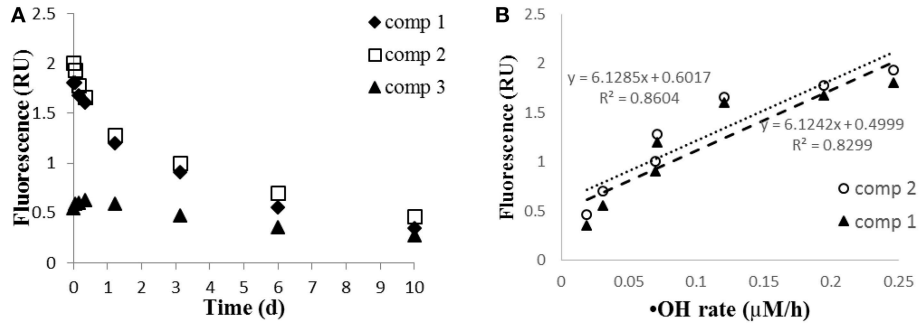

FIGURE 6 | (A) EEMS-PARAFAC components 1 and 2 (humic-like DOM), and component 3 (tryptophan-like DOM) during irradiation; **(B)** relationship of •OH formation rate (μM/h) to components 1 and 2.

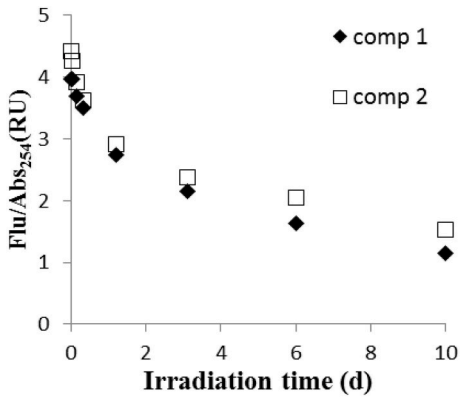

FIGURE 7 | The ratios of fluorescence (Flu) to absorbance at 254 nm (Abs_{254}) for component 1 and 2.

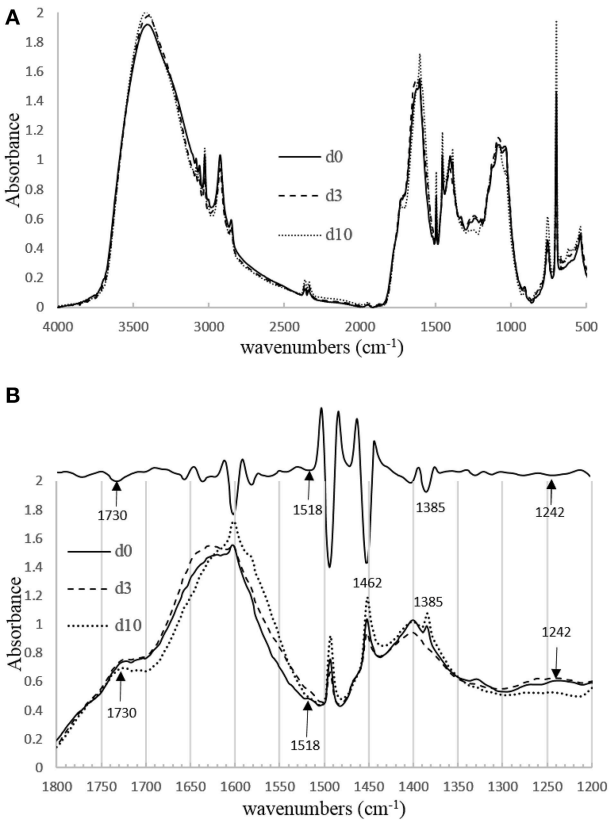

FIGURE 8 | (A) The region between 4000 and 500 cm^{-1} of the FT-IR spectra for the initial wood leachate sample and after 3 and 10 days of irradiation. **(B)** Bottom: The region between 1800 and 1200 cm^{-1} of the FT-IR spectra. Upper: second derivative FT-IR spectrum obtained from day 10 irradiation.

decreased while component 3 did not change significantly during the 10 day irradiation (**Figure 6A**). The decrease of humic-like components during irradiation is consistent with past studies (Ishii and Boyer, 2012; Xu and Jiang, 2013). Also, the results show that the •OH formation rate is positively correlated to humic-like components (component 1 and 2; $R^2 = \sim 0.83$–0.86; **Figure 6B**). The latter result is consistent with Lee et al. (2013) who showed that the •OH apparent quantum yield from the humic fraction in wastewater effluent organic matter was much higher than that from non-humic fraction.

From the ratio of fluorescence (Flu) to absorbance at 254 nm (Abs_{254}) (**Figure 7**), it is clear that humic fluorescence (FDOM) components (components 1 and 2) are 3–4 times more photolabile than most of the other CDOM components. In our sample, humic substances are primarily derived from lignin transformation (Mcdonald et al., 2004). From FT-IR spectroscopy (**Figure 8**), lignin-related structures, which correspond to bands are at 1518 cm^{-1} (vibration of aromatic ring) and 1242 cm^{-1} (C–O asymmetric stretching; Abdulla et al., 2010), decreased during irradiation. Also, the C = O stretching at 1720–1740 cm^{-1} decreased in intensity, indicating the conversion of organic acids into carboxylate and CO_2 (Rodríguez-Zúñiga et al., 2008). In a recent study (Sun et al., 2015b), we reported that simple phenolic acids and related compounds can produce •OH radicals; these phenolic structures are widely present in lignin and humic substances and are thought to be important chromophoric sites within DOM. It should be pointed out that the DOM became progressively more aliphatic during the irradiations, as the bands at 1462 cm^{-1} (CH_3 asymmetric deformation) and 1385 cm^{-1}(CH_3 umbrella mode) increased during irradiation. The increase in aliphatic nature of the DOM will increase its tendency to flocculate during the irradiation (Helms et al., 2013a).

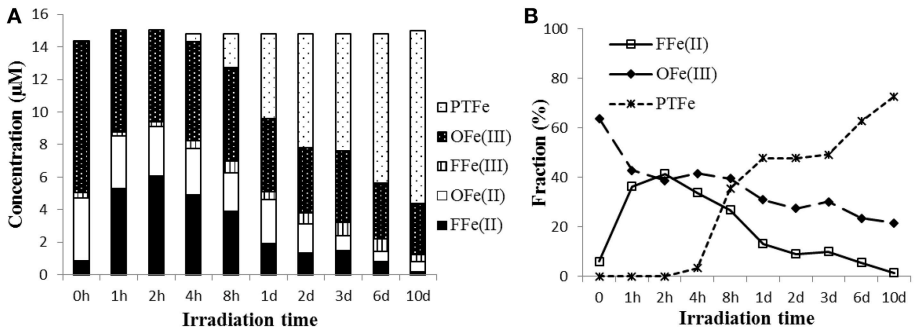

FIGURE 9 | (A) Particulate total Fe (PTFe), DOM-complexed Fe(II) (OFe(II)), DOM-complexed Fe(III) (OFe(III)), free Fe(II) (FFe(II)), free Fe(III) (FFe(III)); **(B)** FFe(II) and OFe(III), and PTFe fraction of TFe (%) in Fe amended aqueous leachate of degraded wood during irradiation. Note non-linearity of the time axis.

Fe Speciation in Fe Amended Wood Leachate

Optical properties were not determined for the Fe amended sample because Fe has a quenching effect on absorbance and fluorescence (Cabaniss, 1992; Pullin et al., 2007; Manciulea et al., 2009) and causes wavelength shifts in FT-IR absorbances (Abdulla et al., 2010). Our Fe speciation results indicate that Fe was initially present mainly as organically complexed Fe(III) in the aqueous phase (**Figure 9A**; Rue and Bruland, 1995; Powell and Wilson-Finelli, 2003). During the initial 2 h of the irradiation, the OFe(III) was partially converted to FFe(II), as evidenced by the drop in the OFe(III) fraction of TFe from 64 to 38%, while the FFe(II) fraction rose from 6 to 41% (**Figure 9B**). These results indicate a reduction of Fe(III) to Fe(II) probably via LMCT processes (Voelker et al., 1997; Klapper et al., 2002; Barbeau, 2006). Thus, Fe was rapidly cycling between Fe(II) and Fe(III) (White et al., 2003; Shiller et al., 2006). Simultaneously, the high •OH formation rate during the first hour (∼1.3 μM/h) and high initial H_2O_2 production (in a similar sample; Sun et al., 2014) indicate that the photo-Fenton reaction was the dominant source for the •OH radical initially.

Because the iron complexed organic ligands were continuously degraded during the irradiation, when the FFe(III) concentration exceeded the maximum soluble concentration, insoluble Fe(III) hydroxide and oxyhydroxides formed, which coprecipitated with and/or adsorbed organic matter. In addition, the Fenton reaction in the Fe amended wood leachate generated substantially more •OH than the sample without added Fe. Therefore, it is likely that •OH played a role in the precipitation of the iron. One may argue that the precipitation was mainly due to an increase of pH, which makes the Fe less soluble during the irradiation. The system initially was buffered by carboxylates but was later buffered by bicarbonate because carboxylates degraded while CO_2 accumulated during the irradiation. However, in our experiment, a pH change was not measurable during the first few hours and thus, initially, it would have had no effect on the observed flocculation. Humic substances within the sample contain high concentrations of hydroxyl and carboxyl groups (**Figure 8**; Sleighter and Hatcher, 2008), which can form strong complexes with Fe. The EEMS and FT-IR results suggest that these structures are preferably degraded, and it appears that the degradation of iron complexing ligands and •OH formation are closely related. This conclusion is supported by Chen et al. (2014), who found the Fe/carbon molar ratios of DOM decreased while this ratio increased for POM using X-ray absorption spectra (XANES and EXAFS).

SUMMARY AND CONCLUSIONS

In the unamended wood leachate sample, DOM was the main source for •OH production, as other sources, such as nitrate and nitrite photolyses and the Fenton reaction, were negligible. The decrease of •OH formation rates normalized to DOC and SUVA indicates that the CDOM sites that produce •OH within DOM are more photolabile than the total DOM fraction. The difference absorbance spectra suggest that these photolabile sites absorb maximally at about 300–310 nm. These sites appear to be located within humic-substances, as supported by the finding that FDOM humic substances are more photolabile than most of the other CDOM components, and are strongly correlated to •OH formation.

In the Fe amended sample, Fe was initially present as mainly dissolved organic complexed Fe(III). During the irradiation, free Fe was released, probably through the photodegradation of Fe complexed organic ligands. When the free Fe(III) concentration exceeded the maximum soluble concentration of Fe(III)(oxy)hydroxides, flocculation occurred. In addition, •OH generated from the Fenton reaction may have played a key role in the precipitation (Waggoner et al., 2015), especially during the early part of the irradiation.

AUTHOR CONTRIBUTIONS

LS conceived, conducted the experiments, interpreted the data and co-wrote the paper. KM conceived the experiments, interpreted the data and co-wrote the paper.

ACKNOWLEDGMENTS

This research was supported by NSF grant OCE0850635 (to KM) awarded through the Chemical Oceanography Program. We thank Drs. Hongmei Chen and Abdulla Hussain for the assistance in sampling, and Anji Chen for assistance in the FT-IR measurements.

REFERENCES

Abdulla, H. A., Minor, E. C., Dias, R. F., and Hatcher, P. G. (2010). Changes in the compound classes of dissolved organic matter along an estuarine transect: a study using FTIR and 13 C NMR. *Geochim. Cosmochim. Acta* 74, 3815–3838. doi: 10.1016/j.gca.2010.04.006

Barbeau, K. (2006). Photochemistry of organic iron (III) complexing ligands in oceanic systems. *Photochem. Photobiol.* 82, 1505–1516. doi: 10.1111/j.1751-1097.2006.tb09806.x

Baruah, M. K., Upreti, M. C., Baishya, N. K., and Dutta, S. N. (1981). Interaction of iron with humic acid extracted from lignite. *Fuel* 60, 971–974. doi: 10.1016/0016-2361(81)90094-6

Buxton, G. V., Greenstock, C. L., Helman, W. P., and Ross, A. B. (1988). Critical review of rate constants for reactions of hydrated electrons, hydrogen atoms and hydroxyl radicals. *Phys. Chem. Ref. Data* 17, 513–886. doi: 10.1063/1.555805

Cabaniss, S. E. (1992). Synchronous fluorescence spectra of metal-fulvic acid complexes. *Environ. Sci. Technol.* 26, 1133–1139. doi: 10.1021/es50002a018

Chen, H., Abdulla, H. A., Sanders, R. L., Myneni, S. C., Mopper, K., and Hatcher, P. G. (2014). Production of black carbon-like and aliphatic molecules from terrestrial dissolved organic matter in the presence of sunlight and iron. *Environ. Sci. Technol. Lett.* 1, 399–404. doi: 10.1021/ez5002598

Emmenegger, L., Schönenberger, R., Sigg, L., and Sulzberger, B. (2001). Light−induced redox cycling of iron in circumneutral lakes. *Limnol. Oceanogr.* 46, 49–61. doi: 10.4319/lo.2001.46.1.0049

Fellman, J. B., Hood, E., and Spencer, R. G. (2010). Fluorescence spectroscopy opens new windows into dissolved organic matter dynamics in freshwater ecosystems: a review. *Limnol. Oceanogr.* 55, 2452–2462. doi: 10.4319/lo.2010.55.6.2452

Gao, H., and Zepp, R. G. (1998). Factors influencing photoreactions of dissolved organic matter in a coastal river of the southeastern United States. *Environ. Sci. Technol.* 32, 2940–2946. doi: 10.1021/es9803660

Guo, W., Yang, L., Hong, H., Stedmon, C. A., Wang, F., Xu, J., et al. (2011). Assessing the dynamics of chromophoric dissolved organic matter in a subtropical estuary using parallel factor analysis. *Mar. Chem.* 124, 125–133. doi: 10.1016/j.marchem.2011.01.003

He, Y.-Y., and Häder, D.-P. (2002). Involvement of reactive oxygen species in the UV-B damage to the cyanobacterium Anabaena sp. *J. Photochem. Photobiol. B Biol.* 66, 73–80. doi: 10.1016/S1011-1344(01)00278-0

Hedges, J. I., and Mann, D. C. (1979). The characterization of plant tissues by their lignin oxidation products. *Geochim. Cosmochim. Acta* 43, 1803–1807. doi: 10.1016/0016-7037(79)90028-0

Helms, J. R., Mao, J., Schmidt-Rohr, K., Abdulla, H., and Mopper, K. (2013a). Photochemical flocculation of terrestrial dissolved organic matter and iron. *Geochim. Cosmochim. Acta* 121, 398–413. doi: 10.1016/j.gca.2013.07.025

Helms, J. R., Mao, J., Stubbins, A., Schmidt-Rohr, K., Spencer, R. G., Hernes, P. J., et al. (2014). Loss of optical and molecular indicators of terrigenous dissolved organic matter during long-term photobleaching. *Aqua. Sci.* 76, 353–373. doi: 10.1007/s00027-014-0340-0

Helms, J. R., Stubbins, A., Perdue, E. M., Green, N. W., Chen, H., and Mopper, K. (2013b). Photochemical bleaching of oceanic dissolved organic matter and its effect on absorption spectral slope and fluorescence. *Mar. Chem.* 155, 81–91. doi: 10.1016/j.marchem.2013.05.015

Helms, J. R., Stubbins, A., Ritchie, J. D., Minor, E. C., Kieber, D. J., and Mopper, K. (2008). Absorption spectral slopes and slope ratios as indicators of molecular weight, source, and photobleaching of chromophoric dissolved organic matter. *Limnol. Oceanogr.* 53:955. doi: 10.4319/lo.2008.53.3.0955

Ishii, S. K. L., and Boyer, T. H. (2012). Behavior of reoccurring PARAFAC components in fluorescent dissolved organic matter in natural and engineered systems: a critical review. *Environ. Sci. Technol.* 46, 2006–2017. doi: 10.1021/es2043504

Kalbitz, K., Solinger, S., Park, J.-H., Michalzik, B., and Matzner, E. (2000). Controls on the dynamics of dissolved organic matter in soils: a review. *Soil Sci.* 165, 277–304. doi: 10.1097/00010694-200004000-00001

Klapper, L., Mcknight, D. M., Fulton, J. R., Blunt-Harris, E. L., Nevin, K. P., Lovley, D. R., et al. (2002). Fulvic acid oxidation state detection using fluorescence spectroscopy. *Environ. Sci. Technol.* 36, 3170–3175. doi: 10.1021/es0109702

Kopáček, J., Klementová, Š., and Norton, S. A. (2005). Photochemical production of ionic and particulate aluminum and iron in lakes. *Environ. Sci. Technol.* 39, 3656–3662. doi: 10.1021/es048101a

Lee, E., Glover, C. M., and Rosario-Ortiz, F. L. (2013). Photochemical formation of hydroxyl radical from effluent organic matter: role of composition. *Environ. Sci. Technol.* 47, 12073–12080. doi: 10.1021/es402491t

Mague, T., Friberg, E., Hughes, D., and Morris, I. (1980). Extracellular release of carbon by marine phytoplankton; a physiological approach. *Limnol. Oceanogr.* 25, 262–279. doi: 10.4319/lo.1980.25.2.0262

Manciulea, A., Baker, A., and Lead, J. R. (2009). A fluorescence quenching study of the interaction of Suwannee River fulvic acid with iron oxide nanoparticles. *Chemos.* 76, 1023–1027. doi: 10.1016/j.chemosphere.2009.04.067

Mcdonald, S., Bishop, A. G., Prenzler, P. D., and Robards, K. (2004). Analytical chemistry of freshwater humic substances. *Anal. Chim. Acta* 527, 105–124. doi: 10.1016/j.aca.2004.10.011

Miller, C. J., Rose, A. L., and Waite, T. D. (2012). Hydroxyl radical production by H2O2-mediated oxidation of Fe (II) complexed by Suwannee River fulvic acid under circumneutral freshwater conditions. *Environ. Sci. Technol.* 47, 829–835. doi: 10.1021/es303876h

Minor, E., Dalzell, B., Stubbins, A., and Mopper, K. (2007). Evaluating the photoalteration of estuarine dissolved organic matter using direct temperature-resolved mass spectrometry and UV-visible spectroscopy. *Aquat. Sci.* 69, 440–455. doi: 10.1007/s00027-007-0897-y

Molot, L. A., Hudson, J. J., Dillon, P. J., and Miller, S. A. (2005). Effect of pH on photo-oxidation of dissolved organic carbon by hydroxyl radicals in a coloured, softwater stream. *Aquat. Sci.* 67, 189–195. doi: 10.1007/s00027-005-0754-9

Mostofa, K. G., Liu, C.-Q., Sakugawa, H., Vione, D., Minakata, D., Saquib, M., et al. (2013). "Photoinduced generation of hydroxyl radical in natural waters," in *Photobiogeochemistry of Organic Matter,* eds K. M. G. Mostofa, T. Yoshioka, A. Mottaleb, and D. Vione (Berlin; Heidelberg: Springer), 209–272.

Murphy, K. R., Butler, K. D., Spencer, R. G., Stedmon, C. A., Boehme, J. R., and Aiken, G. R. (2010). Measurement of dissolved organic matter fluorescence in aquatic environments: an interlaboratory comparison. *Environ. Sci. Technol.* 44, 9405–9412. doi: 10.1021/es102362t

Page, S. E., Arnold, W. A., and Mcneill, K. (2011). Assessing the contribution of free hydroxyl radical in organic matter-sensitized photohydroxylation reactions. *Environ. Sci. Technol.* 45, 2818–2825. doi: 10.1021/es2000694

Powell, R. T., and Wilson-Finelli, A. (2003). Photochemical degradation of organic iron complexing ligands in seawater. *Aquat. Sci.* 65, 367–374. doi: 10.1007/s00027-003-0679-0

Pullin, M. J., Anthony, C., and Maurice, P. A. (2007). Effects of iron on the molecular weight distribution, light absorption, and fluorescence properties of natural organic matter. *Environ. Eng. Sci.* 24, 987–997. doi: 10.1089/ees.2006.0040

Pullin, M. J., Bertilsson, S., Goldstone, J. V., and Voelker, B. M. (2004). Effects of sunlight and hydroxyl radical on dissolved organic matter: bacterial growth efficiency and production of carboxylic acids and other substrates. *Limnol. Oceanogr.* 49, 2011–2022. doi: 10.4319/lo.2004.49.6.2011

Rodríguez-Zúñiga, U. F., Milori, D. M. B. P., da Silva, W. T. L., Martin-Neto, L., Oliveira, L. C., and Rocha, J. C. (2008). Changes in optical properties caused by UV-Irradiation of aquatic humic substances from the amazon river basin: seasonal variability evaluation. *Environ. Sci. Technol.* 42, 1948–1953. doi: 10.1021/es702156n

Rue, E. L., and Bruland, K. W. (1995). Complexation of iron (III) by natural organic ligands in the Central North Pacific as determined by a new competitive ligand equilibration/adsorptive cathodic stripping voltammetric method. *Mar. Chem.* 50, 117–138. doi: 10.1016/0304-4203(95)00031-L

Scott, D. T., McKnight, D. M., Blunt-Harris, E., Kolesar, S., and Lovley, D. (1998). Quinone moieties act as electron acceptors in the reduction of humic substances by humics reducing microorganisms. *Environ. Sci. Technol.* 32, 2984–2989. doi: 10.1021/es980272q

Shiller, A. M., Duan, S., Van Erp, P., and Bianchi, T. S. (2006). Photo−oxidation of dissolved organic matter in river water and its effect on trace element speciation. *Limnol. Oceanogr.* 51, 1716–1728. doi: 10.4319/lo.2006.51.4.1716

Sleighter, R. L., and Hatcher, P. G. (2008). Molecular characterization of dissolved organic matter (DOM) along a river to ocean transect of the lower Chesapeake Bay by ultrahigh resolution electrospray ionization Fourier transform ion

cyclotron resonance mass spectrometry. *Mar. Chem.* 110, 140–152. doi: 10.1016/j.marchem.2008.04.008

Spencer, R. G., Aiken, G. R., Wickland, K. P., Striegl, R. G., and Hernes, P. J. (2008). Seasonal and spatial variability in dissolved organic matter quantity and composition from the Yukon River basin, Alaska. *Global Biogeochem. Cy.* 22:GB4002. doi: 10.1029/2008GB003231

Stedmon, C. A., and Bro, R. (2008). Characterizing dissolved organic matter fluorescence with parallel factor analysis: a tutorial. *Limnol. Oceanogr. Met.* 6, 572–579. doi: 10.4319/lom.2008.6.572

Sun, L., Chen, H., Abdulla, H. A., and Mopper, K. (2014). Estimating hydroxyl radical photochemical formation rates in natural waters during long-term laboratory irradiation experiments. *Env. Sci. Process. Impact* 16, 757–763. doi: 10.1039/C3EM00587A

Sun, L., Qian, J., Blough, N. V., and Mopper, K. (2015b). Insights into the photoproduction sites of hydroxyl radicals by dissolved organic matter in natural waters. *Environ. Sci. Technol. Lett.* 2, 352–356. doi: 10.1021/acs.estlett.5b00294

Sun, L., Spencer, R. G., Hernes, P. J., Dyda, R. Y., and Mopper, K. (2015a). A comparison of a simplified cupric oxide oxidation HPLC method with the traditional GC−MS method for characterization of lignin phenolics in environmental samples. *Limnol. Oceanogr. Met.* 13, 1–8. doi: 10.1002/lom3.10001

Tangen, G., Wickstrøm, T., Lierhagen, S., Vogt, R., and Lund, W. (2002). Fractionation and determination of aluminum and iron in soil water samples using SPE cartridges and ICP-AES. *Environ. Sci. Technol.* 36, 5421–5425. doi: 10.1021/es020077i

Vaughan, P. P., and Blough, N. V. (1998). Photochemical formation of hydroxyl radical by constituents of natural waters. *Environ. Sci. Technol.* 32, 2947–2953. doi: 10.1021/es9710417

Viollier, E., Inglett, P., Hunter, K., Roychoudhury, A., and Van Cappellen, P. (2000). The ferrozine method revisited: Fe (II)/Fe (III) determination in natural waters. *App. Geochem.* 15, 785–790. doi: 10.1016/S0883-2927(99)00097-9

Vione, D., Falletti, G., Maurino, V., Minero, C., Pelizzetti, E., Malandrino, M., et al. (2006). Sources and sinks of hydroxyl radicals upon irradiation of natural water samples. *Environ. Sci. Technol.* 40, 3775–3781. doi: 10.1021/es052206b

Vione, D., Ponzo, M., Bagnus, D., Maurino, V., Minero, C., and Carlotti, M. (2010). Comparison of different probe molecules for the quantification of hydroxyl radicals in aqueous solution. *Environ. Chem. Lett.* 8, 95–100. doi: 10.1007/s10311-008-0197-3

Voelker, B. M., Morel, F. M., and Sulzberger, B. (1997). Iron redox cycling in surface waters: effects of humic substances and light. *Environ. Sci. Technol.* 31, 1004–1011. doi: 10.1021/es9604018

Waggoner, D. C., Chen, H., Willoughby, A. S., and Hatcher, P. G. (2015). Formation of black carbon-like and alicyclic aliphatic compounds by hydroxyl radical initiated degradation of lignin. *Org. Geochem.* 82, 69–76. doi: 10.1016/j.orggeochem.2015.02.007

White, E., Vaughan, P., and Zepp, R. (2003). Role of the photo-Fenton reaction in the production of hydroxyl radicals and photobleaching of colored dissolved organic matter in a coastal river of the southeastern United States. *Aquat. Sci.* 65, 402–414. doi: 10.1007/s00027-003-0675-4

Xu, H., and Jiang, H. (2013). UV-induced photochemical heterogeneity of dissolved and attached organic matter associated with cyanobacterial blooms in a eutrophic freshwater lake. *Wat. Res.* 47, 6506–6515. doi: 10.1016/j.watres.2013.08.021

Yamashita, Y., Jaffé, R., Maie, N., and Tanoue, E. (2008). Assessing the dynamics of dissolved organic matter (DOM) in coastal environments by excitation emission matrix fluorescence and parallel factor analysis (EEM−PARAFAC). *Limnol. Oceanogr.* 53, 1900–1908. doi: 10.4319/lo.2008.53.5.1900

Zepp, R. G., Faust, B. C., and Hoigne, J. (1992). Hydroxyl radical formation in aqueous reactions (pH 3-8) of iron (II) with hydrogen peroxide: the photo-Fenton reaction. *Environ. Sci. Technol.* 26, 313–319. doi: 10.1021/es00026a011

Zhou, X., and Mopper, K. (1990). Determination of photochemically produced hydroxyl radicals in seawater and freshwater. *Mar. Chem.* 30, 71–88. doi: 10.1016/0304-4203(90)90062-H

Zlotnik, I., and Dubinsky, Z. (1989). The effect of light and temperature on DOC excretion by phytoplankton. *Limnol. Oceanogr.* 34, 831–839. doi: 10.4319/lo.1989.34.5.0831

Conflict of Interest Statement: The authors declare that the research was conducted in the absence of any commercial or financial relationships that could be construed as a potential conflict of interest.